A General Framework of Piecewise-Polynomial Mumford-Shah Model for Image Segmentation

Chong Chen, Juelin Leng, and Guoliang Xu

Abstract

Variational models have been widely applied to deal with various image segmentation problems, largely because they are particularly suitable for imposing much geometric or other prior knowledge on the solutions sought. As the images to be segmented become more complicated, for instance, multiple phases, intensity heterogeneity, etc., these models are designed to be more cumbersome. Motivated by this, we propose a general framework of piecewise-polynomial Mumford-Shah model, which is considerably simple and flexible. Our model generalizes the well-known piecewise-constant case, and is almost the simplest framework to apply piecewise polynomials to appropriately approximate the original Mumford-Shah model. The proposed model is well suited to being efficiently solved by the split Bregman iteration algorithm. Experimental results demonstrate that our model has more desirable performance in terms of segmented accuracy, efficiency and robustness, comparing with other variational models in addressing a number of aforementioned challenging segmentation scenarios.

The work of C. Chen was supported by National Natural Science Foundation of China (NSFC) for youth under the grant 11301520. The work of G. Xu was supported in part by NSFC key project under the grant 10990013, NSFC under the grants 11101401, 81173663 and NSFC Funds for Creative Research Groups of China under the grant 11021101.

C. Chen, J. Leng, and G. Xu are with the State Key Laboratory of Scientific and Engineering Computing, Institute of Computational Mathematics and Scientific/Engineering Computing, Academy of Mathematics and Systems Science, Chinese Academy of Sciences, Beijing, 100190, P.R. China. (e-mail: {chench,lengjl,xuguo}@lsec.cc.ac.cn).

Index Terms

Image segmentation, piecewise polynomials, Mumford-Shah model, multiple phases, intensity heterogeneity, split Bregman iteration, variational model.

I. INTRODUCTION

Image segmentation is one of the most important topics arisen in image processing and computer vision. The purpose of image segmentation is to separate the image of interest into regions that belong to different objects in certain meaningful sense. Among various techniques for solving image-segmentation problems, the variational or partial differential equation (PDE) based models have proven to be a category of considerably effective and influential approaches [1]–[9]. Also, many of other effective methods are developed so far, e.g., [10]–[19], etc.

The model introduced in this work is a generalization of the piecewise-constant Mumford-Shah model (PCMS model) [6], [7], and is also an improvement and simplification of the piecewise-smooth Mumford-Shah model (PSMS model) [7]. We first recall these classic variational models based on the thought of Mumford and Shah. Let us define C as a closed contour in image domain $\Omega \subset \mathbb{R}^d$, where $d = 2$ or 3 and $u_0 : \Omega \to \mathbb{R}$ be a given original image to be segmented. The well-known Mumford-Shah model (MS model) for image segmentation is formulated as follows.

$$\mathcal{E}_{\mathrm{MS}}(u, C) = \int_{\Omega} |u_0 - u|^2 \mathrm{d}\mathbf{x} + \mu \int_{\Omega \setminus C} |\nabla u|^2 \mathrm{d}\mathbf{x} + \nu |C|, \tag{1}$$

where both μ and ν are the given nonnegative parameters to trade off the different terms in the total energy, and $|C|$ is the length of contour C, and u is the segmented image that piecewise-smoothly approximates the considered image u_0 in the distinct regions with C as their separated curve [2]. The lack of differentiability of the functional and the complication of discretization of the unknown discontinuity set do not allow us to directly apply the standard optimization methods to obtain the minima of (1). Therefore, one has to resort to the efficient approximation to the formulation of Mumford-Shah functional. The interested readers can be refer to the monograph [20] and the references therein.

The PCMS model is a reduced version of the MS model, which is almost the simplest approximation of it [6]. Assume that the initial image u_0 is segmented into two regions of approximatively piecewise-

constant intensities, namely, $u = c_i$ inside each connected domain Ω_i $(i = 1, 2)$ with C as their boundary. The PCMS model, also called Chan-Vese model, is formulated as the following energy functional.

$$\mathcal{E}_{\mathrm{PCMS}}(c_1, c_2, C) = \lambda_1 \int_{\Omega_1} |u_0 - c_1|^2 \mathrm{d}\mathbf{x} + \lambda_2 \int_{\Omega_2} |u_0 - c_2|^2 \mathrm{d}\mathbf{x} + \nu |C|, \tag{2}$$

where $\nu \geq 0$, and the values of positive parameters λ_1 and λ_2 are often selected to be the same in most of the literatures (see [6], [7], [21]). Note that c_i is the average intensity of u_0 in domain Ω_i for given C. The model (2) performs a two-phase segmentation of u_0. In practice, this model cannot segment well the intensity- or illumination-heterogeneous images, which has been indicated in several literatures (see [8] and references therein).

In order to overcome the difficulties in segmenting the complicated images, such as the multi-phase, the intensity-heterogeneous in the real world, Vese and Chan proposed a multi-phase PCMS model in level set framework, as well as the following PSMS model [7].

$$\begin{aligned} \mathcal{E}_{\mathrm{PSMS}}(u_1, u_2, C) = & \int_{\Omega_1} |u_0 - u_1|^2 \mathrm{d}\mathbf{x} + \int_{\Omega_2} |u_0 - u_2|^2 \mathrm{d}\mathbf{x} \\ & + \mu \int_{\Omega_1} |\nabla u_1|^2 \mathrm{d}\mathbf{x} + \mu \int_{\Omega_2} |\nabla u_2|^2 \mathrm{d}\mathbf{x} + \nu |C|. \end{aligned} \tag{3}$$

For a fixed C, the third and the fourth terms of (3) can be used to smooth u_1 and u_2 inside the regions Ω_1 and Ω_2 (i.e. piecewise-smooth optimal approximations of u_0), respectively. Minimizing (3) with respect to u_i, $i = 1, 2$, by fixed C, one needs to solve the following Euler-Lagrange equations in each iteration.

$$\begin{cases} u_i - u_0 = \mu \Delta u_i, & \text{in } \ \Omega_i, \\ \frac{\partial u_i}{\partial \mathbf{n}} \ = \ 0, & \text{on } \ \partial\Omega_i, \end{cases} \tag{4}$$

where $\mathbf{n}$ is represented as the unit normal vector at the corresponding boundary. Clearly, updating u_i is much more time-consuming compared with updating c_i in minimizing functional (2).

Furthermore, Li et al. presented a region-scalable fitting energy functional (RSF model) for segmentation of intensity-heterogeneous images [8]. The Gaussian kernel function $G_\sigma(\mathbf{x})$ is applied to control the region scalability from small neighbourhoods to the whole image. In what follows the

level set formulation of RSF model is listed.

$$\begin{aligned}\mathcal{F}_{\mathrm{RSF}}(u_1,u_2,\phi) =&\lambda_1\int_\Omega\int_\Omega G_\sigma(\mathbf{x}-\mathbf{y})|u_0(\mathbf{y})-u_1(\mathbf{x})|^2H_1(\phi(\mathbf{y}))\mathrm{d}\mathbf{y}\mathrm{d}\mathbf{x}\\&+\lambda_2\int_\Omega\int_\Omega G_\sigma(\mathbf{x}-\mathbf{y})|u_0(\mathbf{y})-u_2(\mathbf{x})|^2H_2(\phi(\mathbf{y}))\mathrm{d}\mathbf{y}\mathrm{d}\mathbf{x}\\&+\nu\int_\Omega|\nabla H(\phi)|\mathrm{d}\mathbf{x}+\frac{\mu}{2}\int_\Omega||\nabla\phi|-1|^2\mathrm{d}\mathbf{x},\end{aligned}\tag{5}$$

where λ_1 and λ_2 are positive constants, H is represented as the Heaviside function, and $H_1 = H$, $H_2 = 1 - H$. Fixed ϕ, minimizing (5) in terms of u_i, $i = 1, 2$, one can immediately obtain the updating form of u_i as follows.

$$u_i(\mathbf{x}) = \frac{G_\sigma(\mathbf{x}) * (u_0(\mathbf{x})H_i(\mathbf{x}))}{G_\sigma(\mathbf{x}) * H_i(\mathbf{x})},\tag{6}$$

where $*$ denotes the convolution operator. Hence, the convolutions have to be computed in each iteration, which largely increase the computational cost. As shown in the numerical experiments of [8], on the other hand, the RSF model has better performance than the PSMS model and mean shift algorithm [22] for intensity-heterogeneous image segmentation.

To update the contour C (zero level set of ϕ) for minimizing functionals in (2), (3) or (5), a very popular approach, named level set method, can be successfully used to evolve the current contour to desirable position [23]. Moreover, inspired by the thought—restating a non-convex minimization as a convex optimization problem, then seeking the global minima via classical convex optimization methods [24], Goldstein et al. proposed a particularly efficient split Bregman iteration algorithm to resolve the optimization problem of interest [25].

For the purpose of effectively addressing the multi-phase and intensity-heterogenous image segmentation problems, we propose a general framework of piecewise-polynomial Mumford-Shah model (PPMS model). Followed the simple thought of PCMS model, our model applies the piecewise-polynomial optimal approximation. In constructed form, the PPMS model can be regraded as a generalization of the PCMS model from piecewise constants to piecewise polynomials, that also contains the special case of piecewise constants. In addition, the PPMS model is also an improvement and simplification of the existing models of interest. The level set formulation of our model can be easily derived as those of above mentioned models. Instead of applying level set method, we are prone

to utilize the split Bregman iteration to solve the proposed variational model, which possesses the capability of high-efficient computation.

The outline of this paper is organized as follows. In Section II, we first propose the PPMS model. The connections and distinctions with several existing models are elaborated in Section III. In Section IV, the numerical computing of our model is given, followed by some experimental results in Section V. Conclusion and proposals for future research are given in Section VI.

II. Piecewise-Polynomial Mumford-Shah Model

A. Piecewise-Polynomial Based Variational Model

In this section, we propose a general framework of piecewise-polynomial based variational model for image segmentation. In this paper, we mainly concentrate on the 2D image segmentation because the segmentation model presented by us can be straightforwardly generalized to 3D situation. The C separates Ω into two disjoint regions $\Omega_1 := inside(C)$ and $\Omega_2 := outside(C)$. For a nonnegative integer k, we denote by $\mathcal{P}_k(\Omega_i)$ the set of polynomials of total degree k on Ω_i $(i = 1, 2)$. A general polynomial $\psi(\mathbf{x}) \in \mathcal{P}_k(\Omega_i)$, where $\mathbf{x} = (x, y)$, takes the following form

$$\psi(\mathbf{x}) = \sum_{0 \le s+t \le k} c_{\psi,st} x^s y^t, \quad s,\, t \in \mathbb{Z}^+,$$

where $\mathbb{Z}^+$ denotes the set of nonnegative integers. Let us define the coefficient vector of $\psi(\mathbf{x})$ as $\mathbf{C}_\psi := (c_{\psi,00}, c_{\psi,10}, c_{\psi,01}, c_{\psi,11}, \cdots, c_{\psi,0k})^T$. It is well-known that the number of its components is $\frac{(k+1)(k+2)}{2}$ for the polynomial in $\mathcal{P}_k(\Omega_i)$.

Now we consider the following fidelity term

$$\mathcal{E}_0(\mathbf{C}_p, \mathbf{C}_q, C) = \lambda_1 \int_{\Omega_1} |u_0(\mathbf{x}) - p(\mathbf{x})|^2 \mathrm{d}\mathbf{x} + \lambda_2 \int_{\Omega_2} |u_0(\mathbf{x}) - q(\mathbf{x})|^2 \mathrm{d}\mathbf{x}, \tag{7}$$

where λ_1 and λ_2 are both positive parameters, $p(\mathbf{x}) \in \mathcal{P}_k(\Omega_1)$ and $q(\mathbf{x}) \in \mathcal{P}_k(\Omega_2)$ are two polynomials that approximate the image intensities on Ω_1 and Ω_2, respectively. Here we introduce $\mathbf{C}_p$ and $\mathbf{C}_q$ denoting the coefficient vectors of $p(\mathbf{x})$ and $q(\mathbf{x})$, respectively. As in most of region- and edge-based image segmentation models, we impose several regularization terms, like the length of the contour C, onto above fidelity term. Therefore, we present the following variational model

$$\mathcal{E}_{\mathrm{PPMS}}(\mathbf{C}_p, \mathbf{C}_q, C) = \mathcal{E}_0(\mathbf{C}_p, \mathbf{C}_q, C) + |C|. \tag{8}$$

Moreover, if the coefficients of the fidelity term are equal, we define the variational model of interest is isotropic, otherwise, is anisotropic. In our model, the two parameters play a vital role in addressing considerably complex segmentation problems, such as multiple phases, intensity heterogeneity, etc.

B. Level Set Formulation and Minimization

For simplicity of computation, let us consider the level set formulation of the associated variational model. As in level set method, the closed contour C can be denoted by the zero level set of a Lipschitz function $\phi : \Omega \longrightarrow \mathbb{R}$, such that

$$\begin{cases} C = \{\mathbf{x} \in \Omega : \phi(\mathbf{x}) = 0\}, \\ \Omega_1 = \{\mathbf{x} \in \Omega : \phi(\mathbf{x}) > 0\}, \\ \Omega_2 = \{\mathbf{x} \in \Omega : \phi(\mathbf{x}) < 0\}. \end{cases}$$

Let $\bar{H} = 1 - H$. According to [23], we easily obtain the level set formulation of our model

$$\begin{aligned} \mathcal{F}_{\mathrm{PPMS}}(\mathbf{C}_p, \mathbf{C}_q, \phi) &= \lambda_1 \int_\Omega |u_0(\mathbf{x}) - p(\mathbf{x})|^2 H(\phi) \mathrm{d}\mathbf{x} \\ &\quad + \lambda_2 \int_\Omega |u_0(\mathbf{x}) - q(\mathbf{x})|^2 \bar{H}(\phi) \mathrm{d}\mathbf{x} \\ &\quad + \int_\Omega |\nabla H(\phi)| \mathrm{d}\mathbf{x}. \end{aligned} \tag{9}$$

Let $p(\mathbf{x}) = \sum_{0 \le s+t \le k} c_{p,st} x^s y^t$ and $q(\mathbf{x}) = \sum_{0 \le s+t \le k} c_{q,st} x^s y^t$. Using above notations, (9) can be rewritten as

$$\begin{aligned} \mathcal{F}_{\mathrm{PPMS}}(\mathbf{C}_p, \mathbf{C}_q, \phi) &= \lambda_1 \int_\Omega |u_0 - \sum_{0 \le s+t \le k} c_{p,st} x^s y^t|^2 H(\phi) \mathrm{d}\mathbf{x} \\ &\quad + \lambda_2 \int_\Omega |u_0 - \sum_{0 \le s+t \le k} c_{q,st} x^s y^t|^2 \bar{H}(\phi) \mathrm{d}\mathbf{x} \\ &\quad + \int_\Omega |\nabla H(\phi)| \mathrm{d}\mathbf{x}. \end{aligned} \tag{10}$$

To achieve the target of segmentation, we should minimize the energy functional (10) with respect to $\mathbf{C}_p$, $\mathbf{C}_q$ and ϕ. So we first fix ϕ, and minimize (10) with respect to $\mathbf{C}_p$ and $\mathbf{C}_q$. The following equations are obtained

$$\sum_{0 \le s+t \le k} c_{p,st} \int_\Omega x^{s+h} y^{t+r} H(\phi) \mathrm{d}\mathbf{x} = \int_\Omega x^h y^r u_0 H(\phi) \mathrm{d}\mathbf{x}, \tag{11}$$

$$\sum_{0\leq s+t\leq k} c_{q,st}\int_\Omega x^{s+h}y^{t+r}\bar{H}(\phi)\mathrm{d}\mathbf{x} = \int_\Omega x^h y^r u_0\bar{H}(\phi)\mathrm{d}\mathbf{x}, \tag{12}$$

where $0\leq h+r\leq k,\quad h,\, r\in\mathbb{Z}^+$. Finally, minimizing (10) in terms of ϕ by fixed $\mathbf{C}_p$ and $\mathbf{C}_q$, in what follows we obtain a nonlinear PDE

$$\delta(\phi)\Big[\lambda_1|u_0-\sum_{0\leq s+t\leq k} c_{p,st}x^s y^t|^2-\lambda_2|u_0-\sum_{0\leq s+t\leq k} c_{q,st}x^s y^t|^2-\mathrm{div}\Big(\frac{\nabla\phi}{|\nabla\phi|}\Big)\Big]=0. \tag{13}$$

Let

$$A = \begin{pmatrix} \int_\Omega H(\phi)\mathrm{d}\mathbf{x} & \int_\Omega xH(\phi)\mathrm{d}\mathbf{x} & \cdots & \int_\Omega y^k H(\phi)\mathrm{d}\mathbf{x} \\ \int_\Omega xH(\phi)\mathrm{d}\mathbf{x} & \int_\Omega x^2H(\phi)\mathrm{d}\mathbf{x} & \cdots & \int_\Omega xy^k H(\phi)\mathrm{d}\mathbf{x} \\ \vdots & \vdots & \ddots & \vdots \\ \int_\Omega y^k H(\phi)\mathrm{d}\mathbf{x} & \int_\Omega xy^k H(\phi)\mathrm{d}\mathbf{x} & \cdots & \int_\Omega y^{2k}H(\phi)\mathrm{d}\mathbf{x} \end{pmatrix}, \tag{14}$$

$$B = \begin{pmatrix} \int_\Omega \mathrm{d}\mathbf{x} & \int_\Omega x\mathrm{d}\mathbf{x} & \cdots & \int_\Omega y^k\mathrm{d}\mathbf{x} \\ \int_\Omega x\mathrm{d}\mathbf{x} & \int_\Omega x^2\mathrm{d}\mathbf{x} & \cdots & \int_\Omega xy^k\mathrm{d}\mathbf{x} \\ \vdots & \vdots & \ddots & \vdots \\ \int_\Omega y^k\mathrm{d}\mathbf{x} & \int_\Omega xy^k\mathrm{d}\mathbf{x} & \cdots & \int_\Omega y^{2k}\mathrm{d}\mathbf{x} \end{pmatrix}, \tag{15}$$

$$b = \Big(\int_\Omega u_0H(\phi)\mathrm{d}\mathbf{x}, \int_\Omega xu_0H(\phi)\mathrm{d}\mathbf{x}, \cdots, \int_\Omega y^k u_0H(\phi)\mathrm{d}\mathbf{x}\Big)^T, \tag{16}$$

$$b_0 = \Big(\int_\Omega u_0\mathrm{d}\mathbf{x}, \int_\Omega xu_0\mathrm{d}\mathbf{x}, \cdots, \int_\Omega y^k u_0\mathrm{d}\mathbf{x}\Big)^T. \tag{17}$$

Note that (11) and (12) can be respectively translated into a $\frac{(k+1)(k+2)}{2}\times\frac{(k+1)(k+2)}{2}$ linear system as follows.

$$A\mathbf{C}_p = b, \tag{18}$$

$$(B-A)\mathbf{C}_q = b_0-b. \tag{19}$$

Following the formulations of A, B and the property of Grim matrix, we figure out that if the measures of Ω_1 and Ω_2 are nonzero, A and $B-A$ are both positive definite, otherwise, one of them is zero matrix. The latter case dose not segment the original image at all. In practice, hence, both (18) and (19) are always solvable.

Furthermore, we can derive the multi-phase level set formulation of our model as that in [7]. Due to no essential difficulty, here we omit the derivation.

C. Theoretical Analysis

For the purpose of explaining the basic idea of our model, we first assume that the image u_0 to be segmented is distributed by two regions of piecewise-polynomial intensities, namely, two different polynomial functions $p_{inside}(\mathbf{x})$ and $q_{outside}(\mathbf{x})$, which naturally contains the most simple case: piecewise-constant situation (see [6]). Let C_0 be the intersecting contour of the two regions. Then we assume that $u_0 = p_{inside}(\mathbf{x})$ inside C_0, and $u_0 = q_{outside}(\mathbf{x})$ outside C_0. Now we just consider the fidelity term $\mathcal{E}_0(\mathbf{C}_p, \mathbf{C}_q, C)$ of our variational model (8). It is easy to find that if $C = C_0$, then

$$\mathcal{E}_0(\mathbf{C}_{p_{inside}}, \mathbf{C}_{q_{outside}}, C_0) = \min \mathcal{E}_0(\mathbf{C}_p, \mathbf{C}_q, C) = 0. \tag{20}$$

Otherwise $C \neq C_0$, we immediately have $\mathcal{E}_0(\mathbf{C}_p, \mathbf{C}_q, C) > 0$. Therefore, as the contour C is right on the intersecting contour of the two regions, the fidelity term is minimized to the desired result.

In addition, we suppose that u_0 is a form of two regions of piecewise-smooth intensities or more general case. It is obvious that

$$\min_{\psi \in \mathcal{P}_{k_2}(\Omega_i)} \int_{\Omega_i} |u_0(\mathbf{x}) - \psi(\mathbf{x})|^2 \mathrm{d}\mathbf{x} \leq \min_{\psi \in \mathcal{P}_{k_1}(\Omega_i)} \int_{\Omega_i} |u_0(\mathbf{x}) - \psi(\mathbf{x})|^2 \mathrm{d}\mathbf{x}, \tag{21}$$

for $\mathcal{P}_{k_1}(\Omega_i) \subset \mathcal{P}_{k_2}(\Omega_i)$ as $k_1 < k_2$. Using piecewise-polynomial functions to approximate the segmented regions of u_0 is thereby more accurate than just using piecewise-constant case.

III. Connections and Distinctions Among PPMS Model, PCMS Model and PSMS Model

In this section, we show that PPMS model and PSMS model are closely connected to PCMS model. Moreover, we explain that our model is different essentially from the piecewise-polynomial model proposed by Vese in [21].

For ease of explantation, we recall the level set formulations of PPMS model, PCMS model and PSMS model as follows.

PPMS model :

$$\begin{aligned}\mathcal{F}_{\mathrm{PPMS}}(\mathbf{C}_p, \mathbf{C}_q, \phi) &= \lambda_1 \int_\Omega |u_0(\mathbf{x}) - p(\mathbf{x})|^2 H(\phi) \mathrm{d}\mathbf{x} \\ &\quad + \lambda_2 \int_\Omega |u_0(\mathbf{x}) - q(\mathbf{x})|^2 \bar{H}(\phi) \mathrm{d}\mathbf{x} \\ &\quad + \int_\Omega |\nabla H(\phi)| \mathrm{d}\mathbf{x}. \end{aligned} \tag{22}$$

PCMS model :

$$\begin{aligned}\mathcal{F}_{\mathrm{PCMS}}(c_1, c_2, \phi) &= \lambda_1 \int_\Omega |u_0(\mathbf{x}) - c_1|^2 H(\phi) \mathrm{d}\mathbf{x} \\ &\quad + \lambda_2 \int_\Omega |u_0(\mathbf{x}) - c_2|^2 \bar{H}(\phi) \mathrm{d}\mathbf{x} \\ &\quad + \nu \int_\Omega |\nabla H(\phi)| \mathrm{d}\mathbf{x}. \end{aligned} \tag{23}$$

PSMS model :

$$\begin{aligned}\mathcal{F}_{\mathrm{PSMS}}(u_1, u_2, \phi) &= \int_\Omega |u_0(\mathbf{x}) - u_1(\mathbf{x})|^2 H(\phi) \mathrm{d}\mathbf{x} \\ &\quad + \int_\Omega |u_0(\mathbf{x}) - u_2(\mathbf{x})|^2 \bar{H}(\phi) \mathrm{d}\mathbf{x} \\ &\quad + \mu \int_\Omega |\nabla u_1|^2 H(\phi) \mathrm{d}\mathbf{x} \\ &\quad + \mu \int_\Omega |\nabla u_2|^2 \bar{H}(\phi) \mathrm{d}\mathbf{x} \\ &\quad + \nu \int_\Omega |\nabla H(\phi)| \mathrm{d}\mathbf{x}. \end{aligned} \tag{24}$$

It is easy to see that if $p(\mathbf{x}), q(\mathbf{x}) \in \mathcal{P}_0(\Omega_i), i = 1, 2$ in (22), the PPMS model is reduced to the PCMS model. Our model is, hence, the generalization of PCMS model. Naturally, the PCMS model is not as efficient and flexible as our model for image segmentation, which has been demonstrated by a simple experiment in Section V.

On the other hand, the PSMS model is to seek optimal piecewise-smooth approximation to the original image in each separated region, that is implemented by the third and fourth terms in (24). In [21], Vese also proposed a version of piecewise-polynomial approximations followed the formulation of PSMS model. In particular, choosing both u_1 and u_2 to be polynomials, the piecewise-polynomial

form of PSMS model is obtained as follows.

$$\begin{aligned}\tilde{\mathcal{F}}_{\mathrm{PSMS}}(\mathbf{C}_p, \mathbf{C}_q, \phi) &= \int_\Omega |u_0(\mathbf{x}) - p(\mathbf{x})|^2 H(\phi)\mathrm{d}\mathbf{x} \\ &+ \int_\Omega |u_0(\mathbf{x}) - q(\mathbf{x})|^2 \bar{H}(\phi)\mathrm{d}\mathbf{x} \\ &+ \mu \int_\Omega |\nabla p|^2 H(\phi)\mathrm{d}\mathbf{x} \\ &+ \mu \int_\Omega |\nabla q|^2 \bar{H}(\phi)\mathrm{d}\mathbf{x} \\ &+ \nu \int_\Omega |\nabla H(\phi)|\mathrm{d}\mathbf{x}, \end{aligned} \tag{25}$$

where $p(\mathbf{x})$ and $q(\mathbf{x})$ are both polynomials (22). Clearly, this is different essentially from our model. If $\mu = 0$, the PSMS model is reduced to our isotropic PPMS model. Furthermore, taking u_1 and u_2 to be linear polynomials, the piecewise-linear form of PSMS model is obtained which is precisely equivalent to that in [21]. In this case, one can readily discover that the third and fourth terms of (25) have the capability of inducing the u_1 and u_2 to be constants (identically, causing the coefficients of the first-order terms to be zero). If selecting u_1 and u_2 to be constants, the PSMS model is directly reduced to be the isotropic PCMS model.

IV. Numerical Computing

As derived in Subsection II-B, the often used level set method can be applied to solve the proposed piecewise-polynomial based variational model. We briefly list the algorithm as follows.

Algorithm 1. *Level Set Method* for Our PPMS Model

Step 1. Given an initial contour C_0, $0 < \alpha \ll 1$ and an integer $N_0 > 0$. Accordingly, ϕ^0 is given. Compute A_0 by (14). Set $n := 0$.

Step 2. Update $\mathbf{C}_p$ and $\mathbf{C}_q$ by (18) and (19), respectively:

$$\mathbf{C}_p^n = A_n^{-1} b, \tag{26}$$

$$\mathbf{C}_q^n = (B - A_n)^{-1}(b_0 - b). \tag{27}$$

Then p^n and q^n are obtained.

Step 3. Update ϕ:

$$\frac{\partial \phi^{n+1}}{\partial t} = \delta_\epsilon(\phi^n)\Big[\mathrm{div}\Big(\frac{\nabla \phi^n}{|\nabla \phi^n|}\Big) - \lambda_1 |u_0 - \sum_{0\le s+t\le k} c^n_{p,st} x^s y^t|^2 + \lambda_2 |u_0 - \sum_{0\le s+t\le k} c^n_{q,st} x^s y^t|^2\Big], \tag{28}$$

where δ_ϵ is a smooth approximation of Dirac delta function δ. Compute $r_n = \|\phi^{n+1} - \phi^n\|_2$. If $r_n < \alpha$ or $n+1 > N_0$, stop the iteration, otherwise go to the next step.

Step 4. Set $n := n+1$, update A_n by (14), return to Step 2.

The above algorithm is one of the most basis methods to solve various variational models, which is, however, regarded as a little slow method comparing with the state-of-the-art ones in practice. In order to use the higher efficient approach, we first give the following theorem.

Theorem IV.1: For any given fixed $p(\mathbf{x}) \in \mathcal{P}_k(\Omega_1)$, $q(\mathbf{x}) \in \mathcal{P}_k(\Omega_2)$, a global minimizer for $\mathcal{F}(\mathbf{C}_p, \mathbf{C}_q, \cdot)$ can be obtained by solving the following convex optimization problem

$$\min_{0\le\phi\le 1} \Big\{ \int_\Omega |\nabla \phi| \mathrm{d}\mathbf{x} + \int_\Omega (\lambda_1 |u_0(\mathbf{x}) - p(\mathbf{x})|^2 - \lambda_2 |u_0(\mathbf{x}) - q(\mathbf{x})|^2)\phi \mathrm{d}\mathbf{x}\Big\}, \tag{29}$$

and setting $\Omega_1 = \{\mathbf{x} \in \Omega : \phi(\mathbf{x}) \ge \alpha\}$ for $a.e.$ $\alpha \in [0,1]$.

Proof: The proof of this theorem can be easily obtained following the proof trick of the Theorem 2 in [24]. Therefore, here we omit the details for no essential difference of them. ■

According to Theorem IV.1, we can replace the minimization of $\mathcal{F}(\mathbf{C}_p, \mathbf{C}_q, \cdot)$ by the convex optimization problem (29). The split Bregman iteration algorithm can be, hence, applied to resolve the convex optimization [25], [26]. For completeness, in what follows we introduce this method. For ease of description, let

$$g = \lambda_1 |u_0(\mathbf{x}) - p(\mathbf{x})|^2 - \lambda_2 |u_0(\mathbf{x}) - q(\mathbf{x})|^2.$$

Then the minimization problem (29) can be rewritten as

$$\min_{0\le\phi\le 1} J(\phi), \tag{30}$$

where

$$J(\phi) = \int_\Omega |\nabla \phi| \mathrm{d}\mathbf{x} + \int_\Omega g\phi \mathrm{d}\mathbf{x}.$$

Rather than considering the minimization problem (30), we shall treat another optimization problem as follows.

$$\min_{0\leq\phi\leq 1,\mathbf{d}} \Big\{\|\mathbf{d}\|_1 + \int_\Omega g\phi \mathrm{d}\mathbf{x}\Big\}, \quad \text{s.t.} \quad \mathbf{d} = \nabla\phi. \tag{31}$$

The Bregman iteration method can be efficiently used to solve above optimization problem.

$$(\phi^{n+1}, \mathbf{d}^{n+1}) = \arg\min_{0\leq\phi\leq 1,\mathbf{d}} \Big\{\|\mathbf{d}\|_1 + \int_\Omega g\phi \mathrm{d}\mathbf{x} + \frac{\beta}{2}\|\mathbf{d} - \nabla\phi - \mathbf{b}^n\|_2^2\Big\}, \tag{32}$$

$$\mathbf{b}^{n+1} = \mathbf{b}^n + \nabla\phi^{n+1} - \mathbf{d}^{n+1}. \tag{33}$$

In order to resolve (32), we first fix $\mathbf{d} = \mathbf{d}^n$, then obtain the first-order optimality condition with respect to ϕ as follows.

$$\Delta\phi = \frac{g}{\beta} + \mathrm{div}(\mathbf{d}^n - \mathbf{b}^n), \qquad 0 < \phi < 1, \quad \text{in} \quad \Omega. \tag{34}$$

We apply central difference and backward difference to discrete the Laplace operator and divergence operator respectively. The Gauss-Seidel iteration is used to solve the associated linear system [27]. We obtain the following update for ϕ^{n+1} in component form.

$$\phi_{i,j}^{n+1} = \min\{\max\{\omega_{i,j}^{n+1}, 1\}, 0\}, \quad 0 \leq i \leq N_x, \quad 0 \leq j \leq N_y, \tag{35}$$

where $N_x \times N_y$ denotes the size of the original image in pixel grid, and

$$\begin{aligned}
\omega_{i,j}^{n+1} &= \frac{1}{4}(\phi_{i-1,j}^n + \phi_{i+1,j}^n + \phi_{i,j-1}^n + \phi_{i,j+1}^n - \frac{g_{i,j}^n}{\beta} - \rho_{i,j}^n),\\
g_{i,j}^n &= (\lambda_1|u_0 - p^n|^2 - \lambda_2|u_0 - q^n|^2)_{i,j},\\
\rho_{i,j}^n &= d_{x,i,j}^n - d_{x,i-1,j}^n + d_{y,i,j}^n - d_{y,i,j-1}^n + b_{x,i-1,j}^n - b_{x,i,j}^n + b_{y,i,j-1}^n - b_{y,i,j}^n.
\end{aligned}$$

Noting that updating variables on $\partial\Omega$, we can use period boundary condition. Next, fixing $\phi = \phi^{n+1}$, we have the update for $\mathbf{d}^{n+1}$ by shrinkage formula as follows.

$$\mathbf{d}^{n+1} = shrinkage(\mathbf{b}^n + \nabla\phi^{n+1}, \frac{1}{\beta}), \tag{36}$$

where

$$shrinkage(x, \lambda) = \frac{x}{|x|}\max\{|x| - \lambda, 0\}.$$

We summarize the split Bregman iteration algorithm for our PPMS model as follows.

Algorithm 2. *Split Bregman Iteration* for Our PPMS Model

Step 1. Given an initial contour C_0, $\mathbf{b}^0$, $0 < \alpha \ll 1$ and an integer $N_0 > 0$. Correspondingly, ϕ^0 is given. Compute A_0 by (14). Set $n := 0$.

Step 2. Update $\mathbf{C}_p$ and $\mathbf{C}_q$ as (26) and (27), respectively.

Step 3. Update ϕ by (35), and compute $r_n = \|\phi^{n+1} - \phi^n\|_2$. If $r_n < \alpha$ or $n + 1 > N_0$, stop the iteration, otherwise, update $\mathbf{d}$ and $\mathbf{b}$ by (36) and (33) respectively, then go to the next step.

Step 4. Set $n := n + 1$, update A_n by (14), return to Step 2.

As shown in Algorithm 2, the computation for solving convolution or PDE is not required at all. It is easy to figure out that the computational complexity using split Bregman iteration for our model is much less than that for RSF model, and is much fewer than that applying level set method for PSMS model, respectively.

V. Experimental Results

In this section, we present several numerical experiments using synthetic and real images to illustrate that our proposed model can produce desirable performance for image segmentation, especially for the images with characteristics of multiple phases (> 2) or intensity heterogeneity. In practice, we can restrict the proposed PPMS model to be two-phase and piecewise-linear, namely, $p(\mathbf{x}), q(\mathbf{x}) \in \mathcal{P}_1(\Omega_i), i = 1, 2$, respectively. We apply the aforementioned split Bregman iteration method to solve our PPMS model. The algorithm is programmed in C language and all the implementations ran on a laptop of Lenovo W530 with Intel Core i7-3720QM 2.60GHz CPU, Fedora 18 OS and GCC 4.7.2 compiler, and no any parallel computing was involved. The compared models are also solved by the split Bregman iteration algorithm. All of the involved parameters are almost chosen optimally to present the best performance of the considered models.

In Fig. 1, we first show the our model can effectively detect multiple levels (> 2) of distinct intensities from different initial contours using two synthetic images. The selection of related parameters is shown in Table 1. We compare our anisotropic model with the well-known two-phase PCMS model and our isotropic PPMS model. It is obvious that the above two models both cannot address well the segmentation of multi-phase images as shown in Fig. 1. Instead, the desired

contours are all automatically detected by our anisotropic PPMS model. Hence, by choosing different values of parameters λ_1 and λ_2, just applying two-phase and piecewise-linear case of our model can successfully detect multi-phase objects, no matter how we choose the initial contour. Hence, our model is relatively more robust than PCMS model. Although the four-phase PCMS model can produce the same performance as our model, as demonstrated in [7], the computational cost for solving that model is a bit more than that of ours. This is due to the fact that two related energy functionals should be minimized simultaneously for four-phase PCMS model.

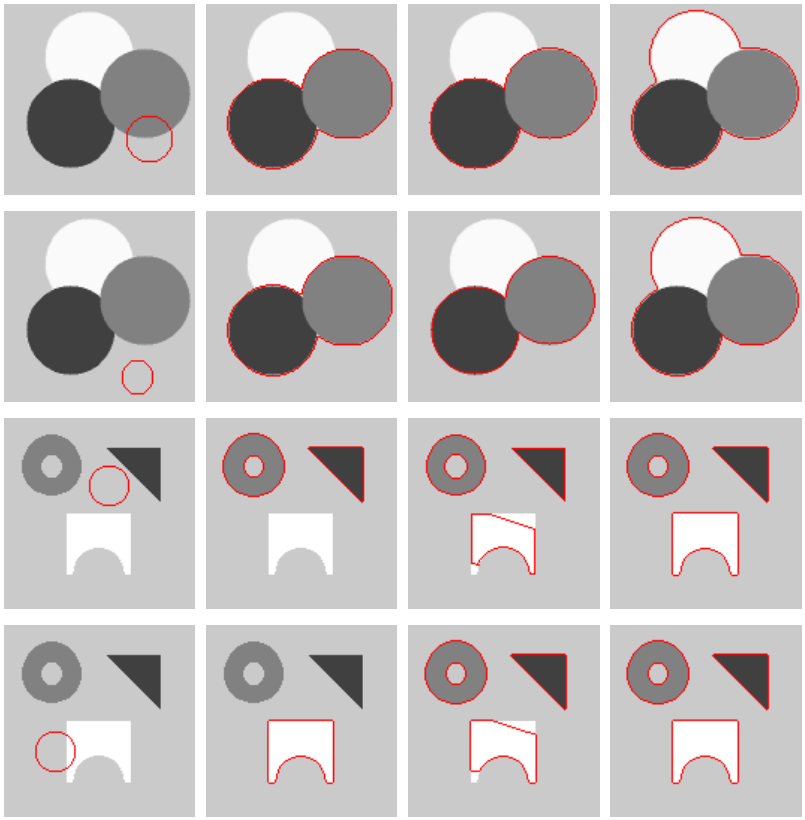

Fig 1. Segmentation of the synthetic images with multiple phases ($= 4$) of distinct intensities. The sizes of the images are both 128×128. The initial contours and the original images (column 1). The final results of two-phase PCMS model (column 2), isotropic PPMS model (column 3) and anisotropic PPMS model (column 4).

In Fig. 2, we show how our model can effectively detect the objects in complicated scenes or intensity-heterogeneous backgrounds. As RSF model has been demonstrated to be more effective than

TABLE 1

THE SELECTION OF PARAMETERS FOR IMAGE SEGMENTATION BY OUR MODEL AND THE PCMS MODEL IN FIG. 1. FROM TOP TO BOTTOM AND LEFT TO RIGHT OF FIG. 1, THE NUMBER OF THE ROWS AND THE COLUMNS IS FROM ROW 1 TO ROW 4 AND COLUMN 1 TO COLUMN 4, RESPECTIVELY.

	Column 2			Column 3			Column 4		
	λ_1	λ_2	β	λ_1	λ_2	β	λ_1	λ_2	β
Row 1	7.5	10	5	1/0.001	1/0.001	5	1/0.04	1/0.001	5
Row 2	5	10	5	1/0.008	1/0.008	0.2	1/0.04	1/0.008	0.2
Row 3	10	20	2	1/0.0005	1/0.0005	5	1/0.05	1/0.005	5
Row 4	15	10	5	1/0.005	1/0.005	5	1/0.0.05	1/0.005	5

PCMS model, PSMS model and mean shift method for the segmentation of intensity-inhomogeneous images [8], now we mainly compare our model with RSF model. Omitting the last term of RSF model, we use split Bregman method to resolve the reduced version as that in [28]. It is worth to noting that ignoring the last term of RSF model is reasonable. Because the level set method being not applied to resolve the RSF model means that the level set initialization needs not to be conducted. In the computational procedure of RSF model, we fix the scale parameter $\sigma = 3$. The image sizes are indicated in Table 2. The selection of the parameters is presented in Table 3. As shown in Fig. 2, from segmented accuracy point of view, our anisotropic model is superior to our isotropic model, and our model has the advantage over RSF model.

Comparing the computational procedures, it is obvious that our model is much simpler and more efficient than RSF model. This is because that the convolutions need to be computed in each iteration for solving RSF model. The least demanded iteration numbers for our model and RSF model to successfully segment the two images are given in column Iter. ♯1 and column Iter. ♯2 of Table 2, respectively. The CPU times in seconds for these segmentations in Fig. 2 are also listed in Table 2. This comparison shows that our model is indeed superior to RSF model in aspect of computational efficiency.

In practice, the medical images are often with intensity heterogeneity due to several objective limitations of current imaging techniques. In this case, we further demonstrate that our model can

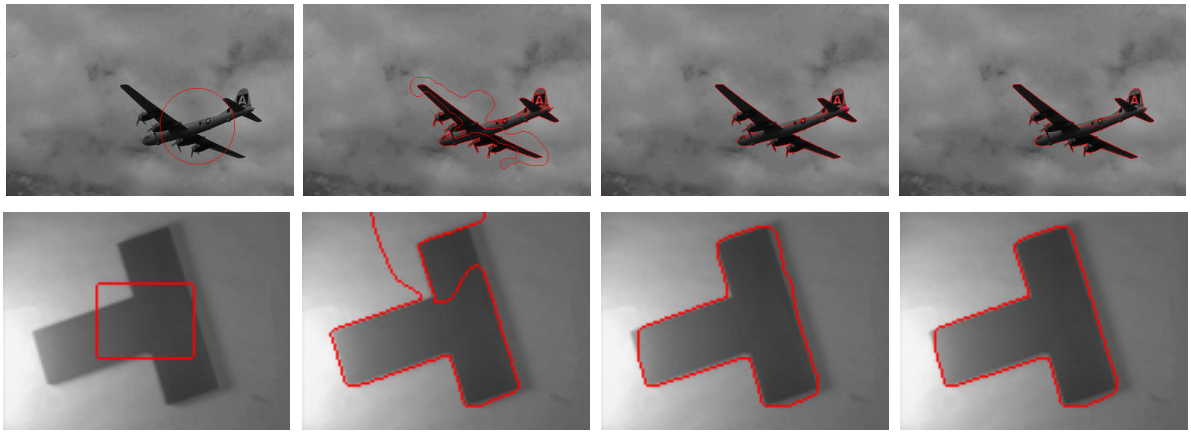

Fig 2. Segmentation of the real images with intensity heterogeneity. The initial contours and the original images (column 1). The final results of RSF model (column 2), isotropic PPMS model (column 3), and anisotropic PPMS model (column 4).

TABLE 2

THE SIZES OF THE IMAGES, THE LEAST DEMANDED ITERATION NUMBERS, THE CPU TIMES IN SECONDS FOR IMAGE SEGMENTATION BY OUR MODEL AND THE RSF MODEL IN FIG. 2. THE ITER. ♯1 AND ITER. ♯2 DENOTE THE LEAST DEMANDED ITERATION NUMBERS FOR OUR MODEL AND RSF MODEL, RESPECTIVELY. FROM TOP TO BOTTOM OF FIG. 2, THE NUMBER OF THE IMAGES IS FROM 1 TO 2.

	Size	Iter. ♯1	Our model	Iter. ♯2	RSF model
Image 1	481×321	50	3.27	50	43.55
Image 2	127×96	40	0.2	40	2.77

yield desirable performance on the medical image segmentation in Fig. 3. By applying the same initial contours and the original images, the segmentation results of RSF model and our isotropic PPMS model for the first and the second images are similar to those of our anisotropic PPMS model. For the third to fifth images, however, RSF model produces a lot of unwanted or error segmentations, and our isotropic PPMS model yields several inaccurate contours. Moreover, the performance of the later is much better than that of the former. It is clear that our anisotropic PPMS model is much more flexible and precise than the compared two models to segment the intensity-heterogeneous images. We choose the related parameters to be almost optimal, which are shown in Table 5.

In addition, the least demanded iteration numbers for our model and RSF model to successfully

TABLE 3

THE SELECTION OF PARAMETERS FOR IMAGE SEGMENTATION BY OUR MODEL AND THE RSF MODEL IN FIG. 2. FROM TOP TO BOTTOM AND LEFT TO RIGHT OF FIG. 2, THE NUMBER OF THE ROWS AND THE COLUMNS IS FROM ROW 1 TO ROW 2 AND COLUMN 1 TO COLUMN 4, RESPECTIVELY.

	Column 2				Column 3			Column 4		
	λ_1	λ_2	$\nu/255^2$	β	λ_1	λ_2	β	λ_1	λ_2	β
Row 1	1	1	0.001	1000	1/0.04	1/0.04	2.5	1/0.06	1/0.045	5.5
Row 2	1	1	0.005	2000	1/0.075	1/0.075	12.5	1/0.03	1/0.045	0.1

segment the five images are listed in column Iter. ♯1 and column Iter. ♯2 of Table 4, respectively. The CPU times in seconds for these segmentations in Fig. 3 are also presented. In terms of computational efficiency, this comparison shows that our model is far more rapidly than RSF model.

TABLE 4

THE SIZES OF THE IMAGES, THE LEAST DEMANDED ITERATION NUMBERS, THE CPU TIMES IN SECONDS FOR IMAGE SEGMENTATION BY OUR MODEL AND THE RSF MODEL IN FIG. 3. THE ITER. ♯1 AND ITER. ♯2 DENOTE THE LEAST DEMANDED ITERATION NUMBERS FOR OUR MODEL AND RSF MODEL, RESPECTIVELY. FROM TOP TO BOTTOM OF FIG. 3, THE NUMBER OF THE IMAGES IS FROM 1 TO 5.

	Size	Iter. ♯1	Our model	Iter. ♯2	RSF model
Image 1	111×110	10	0.05	49	3.36
Image 2	103×131	28	0.15	73	5.56
Image 3	119×78	50	0.19	50	2.62
Image 4	180×107	50	0.4	50	8.81
Image 5	169×207	10	0.15	48	15.52

Finally, we would like to discuss the selection of the almost optimal parameters for our model in this work. Selecting the optimal parameters for variational models is almost ubiquitous, which is of significant importance in practice. Here we have no nice theoretical guideline to choose them. However, we propose a heuristic method: (1) Given an initial λ^0 and θ^0, let $\lambda_1 = \lambda_2 = \lambda^0$ and $\theta = \theta^0$; (2) If the current result is not satisfactory, fixed one parameter λ^0 or θ^0, tune another one

TABLE 5

THE SELECTION OF PARAMETERS FOR IMAGE SEGMENTATION BY OUR MODEL AND THE PCMS MODEL IN FIG. 3. FROM TOP TO BOTTOM AND LEFT TO RIGHT OF FIG. 3, THE NUMBER OF THE ROWS AND THE COLUMNS IS FROM ROW 1 TO ROW 5 AND COLUMN 1 TO COLUMN 4, RESPECTIVELY.

	Column 2				Column 3			Column 4		
	λ_1	λ_2	$\nu/255^2$	β	λ_1	λ_2	β	λ_1	λ_2	β
Row 1	1.1	1	0.001	300	1/0.005	1/0.005	1.5	1/0.005	1/0.005	1.5
Row 2	1	1	0.008	80	1/0.005	1/0.005	5.5	1/0.005	1/0.005	5.5
Row 3	1	2	0.0015	1080	1/0.04	1/0.04	20	1/0.025	1/0.046	20
Row 4	1.6	1	0.0013	3000	1/0.006	1/0.006	5	1/0.022	1/0.005	5
Row 5	1	1.15	0.0025	1400	1/0.005	1/0.005	5	1/0.0014	1/0.005	5

to obtain an improved result. Then we get two better parameters λ^1 and θ^1; (3) If the improved result is not acceptable yet, we try to change one of λ_1 and λ_2. If the result of $\lambda_1 > \lambda_2$ becomes bad, we immediately let $\lambda_1 < \lambda_2$. Then we obtain a better performance with parameters λ^2, λ^3 and θ^1; (4) If necessary, we could make a proportionate change on the values of λ^2 and λ^3 to get the optimal parameters. In practice, we need not to execute the entire steps of above method. As analyzed the results of selecting parameters of Fig. 1–3, we can figure out that the optimal parameters are almost within several focusing intervals. Since it is relatively easy to select the approximating optimal parameters for our model.

VI. CONCLUSION AND FUTURE WORK

We have introduced a new piecewise-polynomial Mumford-Shah model for image segmentation. Our model contains the classic Chan-Vese model, and is almost the simplest framework to apply piecewise polynomials to appropriately approximate the original Mumford-Shah model. Particularly, in piecewise-linear and two-phase case, the proposed model is capable of producing accurate contours to segment the synthetic and real images with multiple phases or intensity heterogeneity. In addition, instead of the conventional level set method, the split Bregman iteration algorithm is well suited to efficiently resolving the proposed model. The large-scale images can be, therefore, considerably

fast segmented by our model. Experimental results have shown that the proposed model has more desirable performance in terms of segmented accuracy, efficiency and robustness than several classic variational segmentation models. The general framework has much improved the performances and greatly simplified formulations of the models designed to address above challenging segmentation problems.

It is worth noting that the parameters λ_1 and λ_2 in our model play a key role in accurately segmenting the complicated images. Based on the numerical experiments, we speculate that a theoretical relationship between them may exist. In future work, we will explore the intrinsic connections between the parameters λ_1, λ_2 and the properties of the original images and the initial contours, which is of greatly practical significance for designing automatically segmentation software. In this article, we just apply the piecewise-linear case to implement the experiments. So how about the higher order situation? Future work, therefore, also includes the investigation on selecting the appropriate degrees of the used piecewise polynomials.

REFERENCES

[1] M. Kass, A. Witkin, and D. Terzopoulos, "Snakes: Active contour models," *International Journal of Computer Vision*, vol. 1, no. 4, pp. 321–331, 1988.

[2] D. Mumford and J. Shah, "Optimal approximations by piecewise smooth functions and associated variational problems," *Communications on Pure and Applied Mathematics*, vol. 42, no. 5, pp. 577–685, 1989.

[3] J. M. Morel and S. Solimini, *Variational methods in image segmentation*. Birkhauser Boston, 1995.

[4] S. Kichenassamy, A. Kumar, P. Olver, A. Tannenbaum, and A. Yezzi, "Gradient flows and geometric active contour models," in *Computer Vision, 1995 Proceedings Fifth International Conference on*. IEEE, 1995, pp. 810–815.

[5] V. Caselles, R. Kimmel, and G. Sapiro, "Geodesic active contours," *International Journal of Computer Vision*, vol. 22, no. 1, pp. 61–79, 1997.

[6] T. F. Chan and L. A. Vese, "Active contours without edges," *Image Processing, IEEE Transactions on*, vol. 10, no. 2, pp. 266–277, 2001.

[7] L. A. Vese and T. F. Chan, "A multiphase level set framework for image segmentation using the Mumford and Shah model," *International Journal of Computer Vision*, vol. 50, no. 3, pp. 271–293, 2002.

[8] C. Li, C.-Y. Kao, J. C. Gore, and Z. Ding, "Minimization of region-scalable fitting energy for image segmentation," *Image Processing, IEEE Transactions on*, vol. 17, no. 10, pp. 1940–1949, 2008.

[9] J. Ye and G. Xu, "Geometric flow approach for region-based image segmentation," *Image Processing, IEEE Transactions on*, vol. 21, no. 12, pp. 4735–4745, 2012.

[10] R. M. Haralick and L. G. Shapiro, "Image segmentation techniques," *Computer Vision, Graphics, and Image Processing*, vol. 29, no. 1, pp. 100–132, 1985.

[11] C. A. Bouman and M. Shapiro, "A multiscale random field model for Bayesian image segmentation," *Image Processing, IEEE Transactions on*, vol. 3, no. 2, pp. 162–177, 1994.

[12] D. K. Panjwani and G. Healey, "Markov random field models for unsupervised segmentation of textured color images," *Pattern Analysis and Machine Intelligence, IEEE Transactions on*, vol. 17, no. 10, pp. 939–954, 1995.

[13] S. C. Zhu and A. Yuille, "Region competition: Unifying snakes, region growing, and Bayes/MDL for multiband image segmentation," *Pattern Analysis and Machine Intelligence, IEEE Transactions on*, vol. 18, no. 9, pp. 884–900, 1996.

[14] K. Held, E. R. Kops, B. J. Krause, W. M. Wells III, R. Kikinis, and H.-W. Muller-Gartner, "Markov random field segmentation of brain MR images," *Medical Imaging, IEEE Transactions on*, vol. 16, no. 6, pp. 878–886, 1997.

[15] J. Shi and J. Malik, "Normalized cuts and image segmentation," *Pattern Analysis and Machine Intelligence, IEEE Transactions on*, vol. 22, no. 8, pp. 888–905, 2000.

[16] Y. Zhang, M. Brady, and S. Smith, "Segmentation of brain MR images through a hidden Markov random field model and the expectation-maximization algorithm," *Medical Imaging, IEEE Transactions on*, vol. 20, no. 1, pp. 45–57, 2001.

[17] P. F. Felzenszwalb and D. P. Huttenlocher, "Efficient graph-based image segmentation," *International Journal of Computer Vision*, vol. 59, no. 2, pp. 167–181, 2004.

[18] D. Freedman and T. Zhang, "Interactive graph cut based segmentation with shape priors," in *Computer Vision and Pattern Recognition, 2005. CVPR 2005. IEEE Computer Society Conference on*, vol. 1. IEEE, 2005, pp. 755–762.

[19] Y. Boykov and G. Funka-Lea, "Graph cuts and efficient ND image segmentation," *International Journal of Computer Vision*, vol. 70, no. 2, pp. 109–131, 2006.

[20] G. Aubert and P. Kornprobst, *Mathematical problems in image processing: partial differential equations and the calculus of variations*. Springer, 2006, vol. 147.

[21] L. Vese, "Multiphase object detection and image segmentation," in *Geometric Level Set Methods in Imaging, Vision, and Graphics*. Springer, 2003, pp. 175–194.

[22] D. Comaniciu and P. Meer, "Mean shift: A robust approach toward feature space analysis," *Pattern Analysis and Machine Intelligence, IEEE Transactions on*, vol. 24, no. 5, pp. 603–619, 2002.

[23] S. Osher and R. Fedkiw, *Level set methods and dynamic implicit surfaces*. Springer, 2003, vol. 153.

[24] T. F. Chan, S. Esedoglu, and M. Nikolova, "Algorithms for finding global minimizers of image segmentation and denoising models," *SIAM Journal on Applied Mathematics*, vol. 66, no. 5, pp. 1632–1648, 2006.

[25] T. Goldstein, X. Bresson, and S. Osher, "Geometric applications of the split Bregman method: segmentation and surface reconstruction," *Journal of Scientific Computing*, vol. 45, no. 1-3, pp. 272–293, 2010.

[26] T. Goldstein and S. Osher, "The split Bregman method for L1-regularized problems," *SIAM Journal on Imaging Sciences*, vol. 2, no. 2, pp. 323–343, 2009.

[27] G. H. Golub and C. F. Van Loan, *Matrix computations*. JHU Press, 2012, vol. 3.

[28] Y. Yang, C. Li, C.-Y. Kao, and S. Osher, "Split Bregman method for minimization of region-scalable fitting energy for image segmentation," in *Advances in Visual Computing*. Springer, 2010, pp. 117–128.

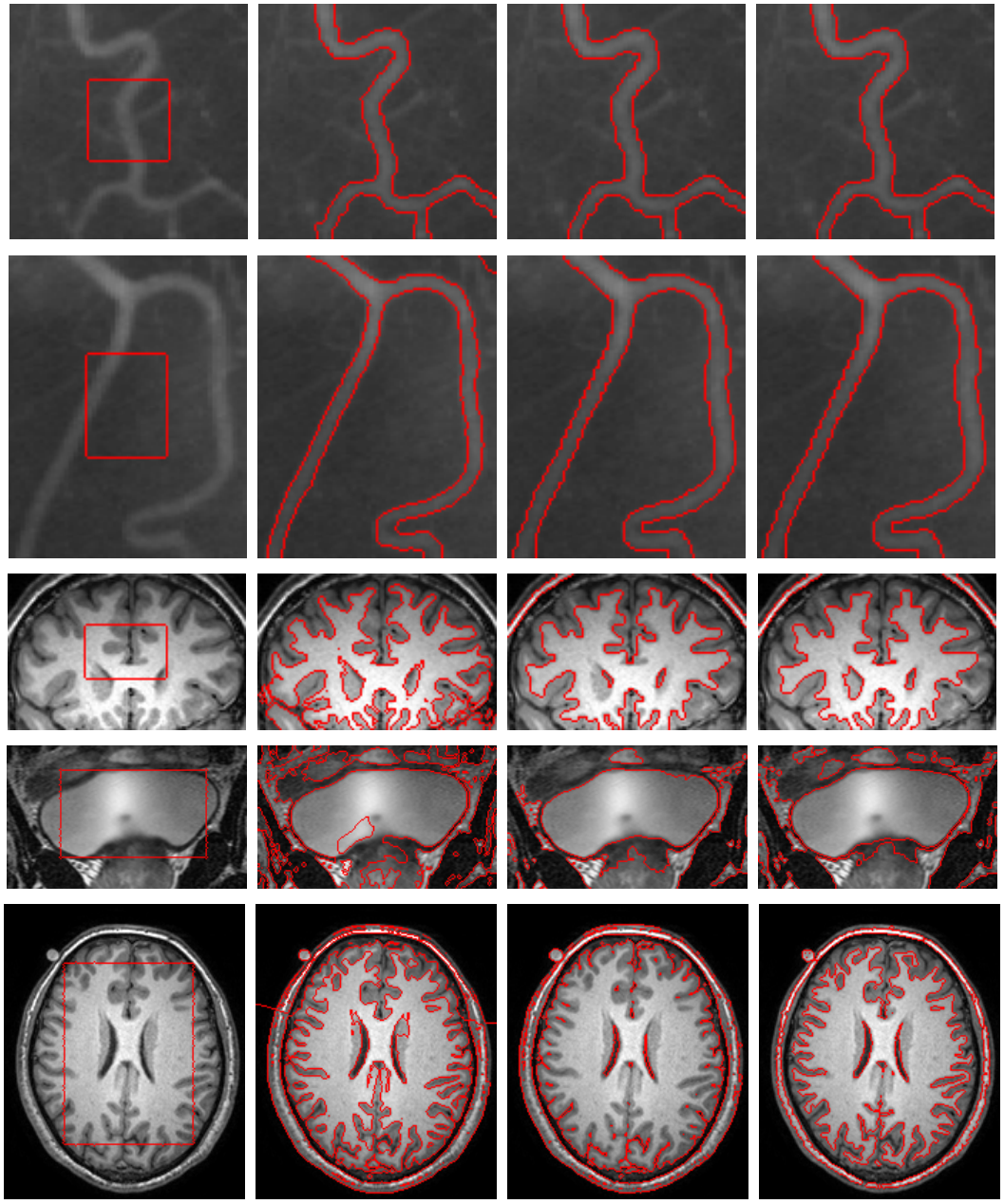

Fig 3. Segmentation of the medical images with intensity heterogeneity. The initial contours and the original images (column 1). The final results of RSF model (column 2), isotropic PPMS model (column3), and anisotropic PPMS model (column 4).